Development of Metallic Sensory Alloys

T. Wallace and J. Newman
NASA Langley Research Center, Hampton, VA, USA

M. Horne
National Institute of Aerospace, Hampton, VA, USA

P. Messick
ATK, Hampton, VA, USA

Keywords: Ferromagnetic Shape Memory Materials, Nondestructive Evaluation (NDE)

Abstract

Existing nondestructive evaluation (NDE) technologies are inherently limited by the physical response of the structural material being inspected and are therefore not generally effective at the identification of small discontinuities, making the detection of incipient damage extremely difficult. One innovative solution to this problem is to enhance or complement the NDE signature of structural materials to dramatically improve the ability of existing NDE tools to detect damage. To address this need, a multifunctional metallic material has been developed that can be used in structural applications. The material is processed to contain second phase sensory particles that significantly improve the NDE response, enhancing the ability of conventional NDE techniques to detect incipient damage both during and after flight. Ferromagnetic shape-memory alloys (FSMAs) are an ideal material for these sensory particles as they undergo a uniform and repeatable change in both magnetic properties and crystallographic structure (martensitic transformation) when subjected to strain and/or temperature changes which can be detected using conventional NDE techniques. In this study, the use of a ferromagnetic shape memory alloy (FSMA) as the sensory particles was investigated.

Introduction

The safety of aerospace vehicles is largely dependent on the ability of modern nondestructive evaluation (NDE) tools to detect structural damage before it reaches a critical size. However, the effectiveness of existing NDE tools requires the identification of small discontinuities using tools such as Eddy current probes, making the detection of incipient damage extremely difficult. Also, the types of NDE tools that can be used are constrained by the physics of the structural material. Thus, the objective of the present study is to develop a multifunctional metallic material that can be used in structural applications but that also contains second phase sensory particles that significantly enhance the ability of conventional NDE techniques to detect incipient damage during flight and at regularly scheduled vehicle inspections.

Ferromagnetic shape-memory alloys (FSMAs) are an ideal material for sensory materials as they undergo a uniform and repeatable change in both magnetic properties and crystallographic structure when subjected to not only temperature changes but also applied strain

[1-2]. This shape-memory behavior is based on martensitic transformations, a diffusionless and reversible transformation between a high-temperature austenite phase and the lower-temperature martensitic phase [1]. As the martensitic transformation is produced by a rapid twinning-like deformation [1], the shape memory material generates an acoustic emission (AE) signal that is orders of magnitude greater than the signature generated by the structural material without shape memory consituents. In addition, FSMAs transition from paramagnetic at higher temperatures to ferromagnetic at lower temperatures when cooled through the Curie temperature (T_c), producing a change in magnetic permeability which can be easily measured. As the Curie temperature has been shown to increase with applied strain [2], evaluating the magnetic properties will provide an additional means of enhancing damage detection with traditional NDE methods, and can also be used for ground-based or in-flight inspection.

A multifunctional metallic material has been produced by embedding the sensory material particles within an alloy to form a "sensory alloy" that could than be used in aerospace structural applications. One application of this multifunctional metallic material would be to detect growing cracks by monitoring the change in properties that are produced by the localized strain around a crack tip. This concept of enhanced crack detection is shown schematically in Figure 1; here, ferromagnetic shape memory material particles are embedded within a structural alloy. In this case, the high strain field in the crack tip process zone results in the changes in the particle magnetic properties and an AE response produced by the austenite-to-martensite phase transformation.

In this study, the crack detection sensory alloy concept was explored. Details will be presented on the development of the sensory material and particles, incorporation of the sensory particles into a structural alloy matrix, and evaluation of the resulting sensory alloy.

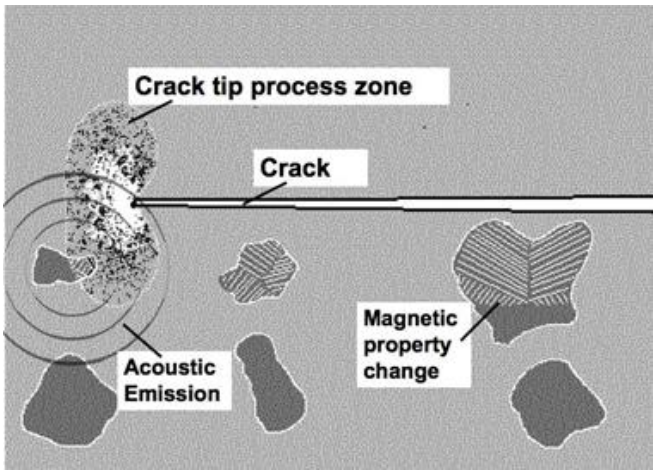

Figure 1 - Schematic of sensory alloy crack detection concept.

Background

Numerous FSMA systems have been investigated for use in other applications, including the CoNiAl [3-6], Ni_2MnGa [7-9], Ni_2MnAl [10-12], FePd [13-14] and Fe_3Pt [15] systems. The temperature and strain dependence of these transformations are a function of the sensory material composition, ambient temperature and applied strain. By carefully choosing the composition of

the FSMA, an alloy can be chosen that will transform under a pre-determined level of strain for a particular application temperature.

For a given composition, the transition is not only dependent upon temperature, but also on applied strain. Therefore, for this application, the martensitic transformation is used to signal that some pre-determined critical strain has been reached at a prescribed temperature. Figure 2 is a schematic of how the transformation temperatures would be expected to vary as a function of applied strain and chemistry. In this figure, the transformation temperatures are labeled as M_s and M_f, or martensite start and finish temperature when the material transforms from austenite to martensite upon cooling, and A_s and A_f, or austenite start and finish temperatures when the material reverts from martensite to austenite when heated. Careful tuning of the composition will give a sensory alloy that will be austenitic at the desired application temperature over a range of applied strains, but at a pre-defined critical strain the transformation temperature will increase to the application temperature and the alloy will transform to martensite. A pseudo elastic material is depicted in Figure 2a. Here, the material is in the austenitic phase at zero strain, and upon loading the material is transformed to the martensitic phase. However, when unloaded the material is transformed back to the austenitic phase. A pseudo elastic material can be used with an on-board sensor, but because the phase change is reversible with applied load, a ground-based inspection would not detect any damage after the structure has been unloaded. However, if the chemistry is selected to be consistent with the behavior depicted in Figure 2b, the material transformed to martensite upon loading will remain as martensite upon unloading.

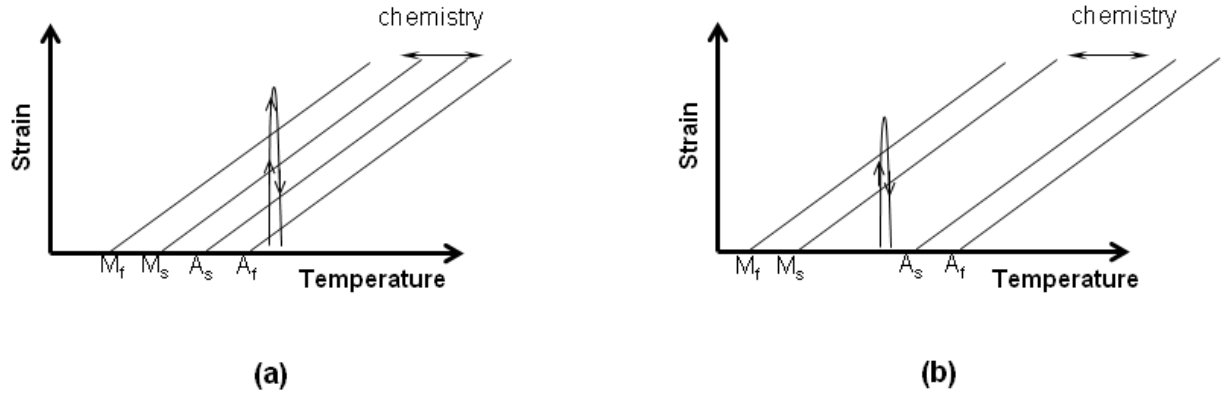

Figure 2 - Relationship between strain and martensite transformation temperature showing a) $T > A_f$ and b) $T < A_s$.

Similarly, for FSMAs the transition between the ferromagnetic and paramagnetic states is is also dependent on both temperature and applied strain as the Curie temperature (the temperature above which a ferromagnetic material reverts to the paramagnetic state) is increased by the resulting deformation. As ferromagnetic materials can have permeability many orders of magnitude greater than paramagnetic materials, there is a change in the magnetic permeability of the FSMA when the magnetic state changes. To measure this effect, one can use a giant magneto resistance (GMR) sensor as a magnetometer to measure the change in the magnetic field strength at a point in the magnetic field near the specimen as the field contracts due to the change from para- to ferro- magnetic state. These industrially available sensors change resistance in the presence of a magnetic field and "giant" refers to the amount of the change compared to other materials with similar behavior.

The composition and processing of the ferromagnetic shape-memory material is critical to the successful development of the sensory alloy. Compositions of the shape-memory materials are classified as types I, II, or III based upon relative positions of martensitic start temperature (M_s) and Curie temperatures of austenite and martensite. Figure 3 shows the variation of M_s and T_c with composition for a typical ferromagnetic shape memory material. As illustrated in this figure, for Type I alloys M_s is higher than T_c, and for Type III alloys, the reverse is true. Thus, Type II alloys (the narrow middle range) are most appropriate for use in this sensory application as the phase change and magnetic change are nearly coincident making it possible to identify both transformations for the same applied strain.

There are three aspects to this innovation: (1) development of the sensory material composition and particles, (2) development of a processing method for incorporation of the sensory material particles within a structural material, and (3) correlation of the sensory material response to an easily detectible signature.

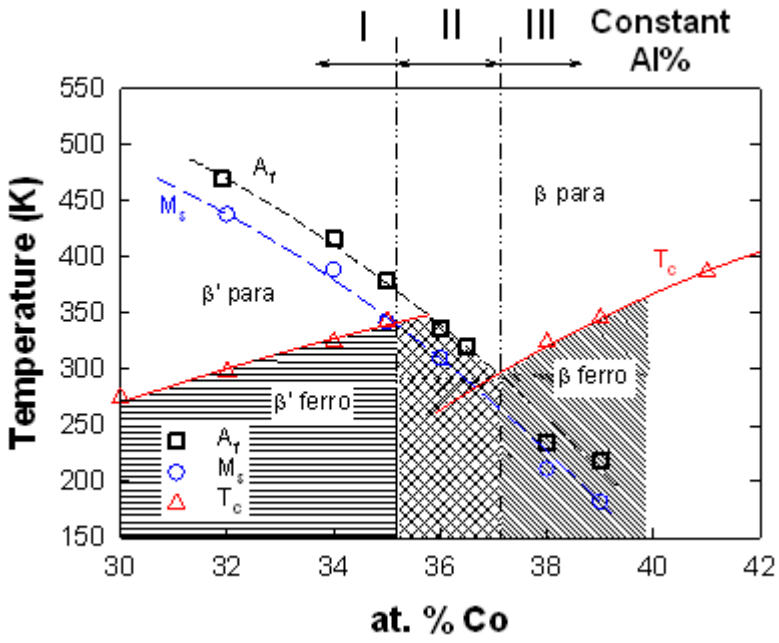

Figure 3 - Schematic of temperature and composition dependence of both martensite transformation temperatures (A_f and M_s) and Curie temperature (T_c) for a CoNiAl FSMA.

Experimental Procedures

Development of Sensory Particles

The temperature and strain dependence of FSMA transformations are dependent on the sensory material composition, ambient temperature and applied strain. By carefully choosing the composition of the FSMA, an alloy can be chosen that will transform under a pre-determined level of strain for a particular application temperature.

Bulk FSMA material has been produced using two methods. In the first method, small quantites (~ 10 g) of FSMA material were prepared using an arc-melter. Here, constituent elements were melted by passing electrical current through the material in an inert environment.

In the second method, larger quantities (~ 1 kg) were fabricated using an induction furnace. Here, constituent elements were melted in a crucible and poured into a casting in an inert environment. The FSMA material was solution-treated in an inert environment followed by a quench in an inert cryogenic pool to retain the high-temperature austenite phase.

While the bulk FSMA product are adequate for examining the behavior of the FSMAs, small particles had to be produced for the creation of the sensory materials. Here, the bulk FSMAs were either mechanically fragmented or processed using gas atomization prior to solution heat treating and quenching. Once in powder form, the quenched FSMAs are ready for incorporation into a sensory material alloy.

Incorporation of Sensory Particles

The sensory alloy was fabricated by mixing the sensory particles with aluminum powder and then consolidating them into a panel for mechanical testing. Two approaches were evaluated for consolidation 1) hot rolling and 2) vacuum hot pressing. For the hot rolling process, the material (FSMA particles plus matrix powder) was placed in an evacuated nonreactive foil bag, heated to a working temperature, and run between two cyclindrial rollers. For the vacuum hot press process, the material was pressed between two plattens at high temperature in vacuum and pressure was applied. Both processes produced panels for mechanical testing having dimensions of approximately 115 mm by 90 mm and a thickness of nearly 2.5 mm. For the results presented in this paper, particles were embedded in a pure aluminum matrix. However, this approach can be used for structural alloys as well.

Evaluation of the Shape Memory Behavior

Shape memory transition temperatures were determined by differential scanning calorimetry (DSC). Scans were conducted over the temperature range of -180^{o}C to 300^{o}C at a scan rate of 10^{o}C/min, and samples were heated and cooled through the test temperature range three times. Martensite start and finish temperatures (M_s and M_f) were determined during the cooling cycles and austenite start and finish temperatures (A_s and A_f) were determined duirng the heating cycles.

The NDE signals of both the sensory material and final sensory alloys were determined in response to increasing strains using both AE and GMR sensors. Small specimens approximately 2.54 mm in diameter and 1.4 mm tall were machined using electro discharge machining (EDM) and strained in compression between cone shaped steel compression platens in a screw driven load frame at a constant displacement rate. An AE sensor was attached to the platens to measure the AE signal during the compressions test. The compression test setup is shown schematically in Figure 4. The platens were wrapped with copper wire as coils to generate a magnetic field that is coupled through the specimen by the platens. A GMR sensor was used as a magnetometer to measure the change in the magnetic field strength at a point in the magnetic field near the specimen as the field contracted due to the change from para- to ferro- magnetic state. This change occurred in our current test setup shown in Figure 4 where the magnetic field between the tips of the platens distorted when the FSMA specimen becomes ferromagnetic.

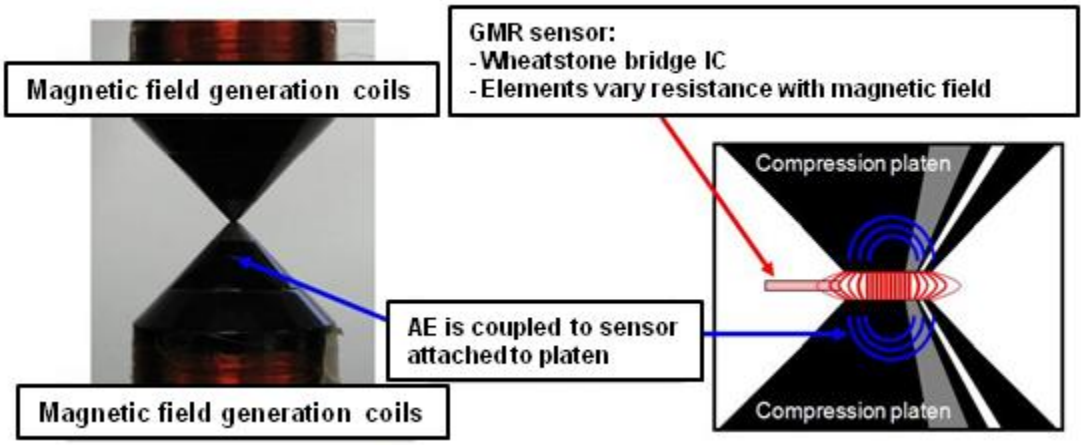

Figure 4 - Compression testing of FSMA pellets.

Mechanical Testing

The tensile and fatigue properties of the sensory alloys were examined to ensure that the mechanical performance was not adversely affected by the presence of the sensory particles. For this purpose, mechanical test specimens were machined from the aluminum panels in accordance with American Society for Testing and Materials (ASTM) standard E 466 [16], as shown in Figure 5. Three or four specimens were machined from each panel. Tensile tests and stress-based fatigue-life tests were conducted with the specimens, as described in the following sections. Panels used for study were produced with the vacuum hot press method, processed with either a 15 minute or 60 minute consolidation time, some containing particles and some without.

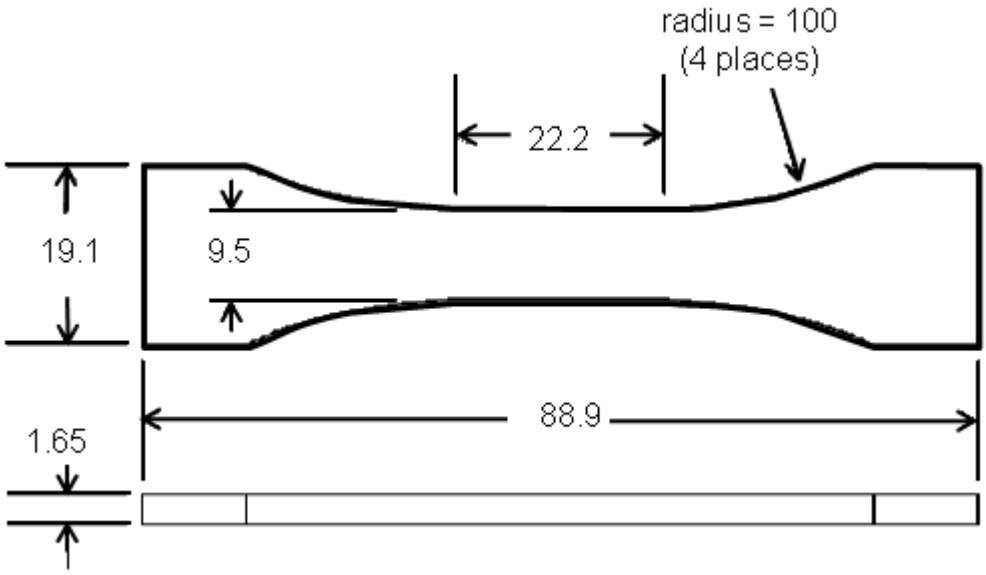

Figure 5 - Specimen configuration (dimensions shown in mm).

Tensile tests were performed in accordance with ASTM standard E 8 [17]. Specimens were gripped at the ends using hydraulic wedge grips in a servo-hydraulic test machine and loaded at a displacement rate of 0.5 mm per minute. Two displacement gages were mounted to opposite sides of the specimen. The initial gage length was 22.2 mm, and engineering strain was computed in accordance with standard test practices of ASTM standard E 8. During tensile testing, load and strain data were acquired every 0.5 seconds (approx. every 4 μm).

Fatigue testing was performed in accordance with ASTM standard E 466. Specimens were gripped at the ends in a servo-hydraulic test machine while sinusoidal constant-amplitude loading was applied at a load ratio (minimum load/maximum load) of R = 0.1 and a loading frequency of 5 Hz until failure occurred. The maximum loads for these tests were defined by the results of the tensile testing.

Results and Discussion

Development of Sensory Particles

Buttons of candidate FSMA compositions fabricated using the arc-melter were solution-treated and quenched, machined into specimens, and then evaluated using DSC to determine the shape-memory transition temperatures. The candidate compositions were found to have M_s temperatures ranging from -150°C to +150°C, and A_f temperatures ranging from -60°C to +200°C. A representative DSC result is presented in Figure 6 for one candidate composition showing both the measured M_s and A_f temperatures. Based on these results a composition was selected that had attractive M_s and A_f temperatures and a larger quantity was produced.

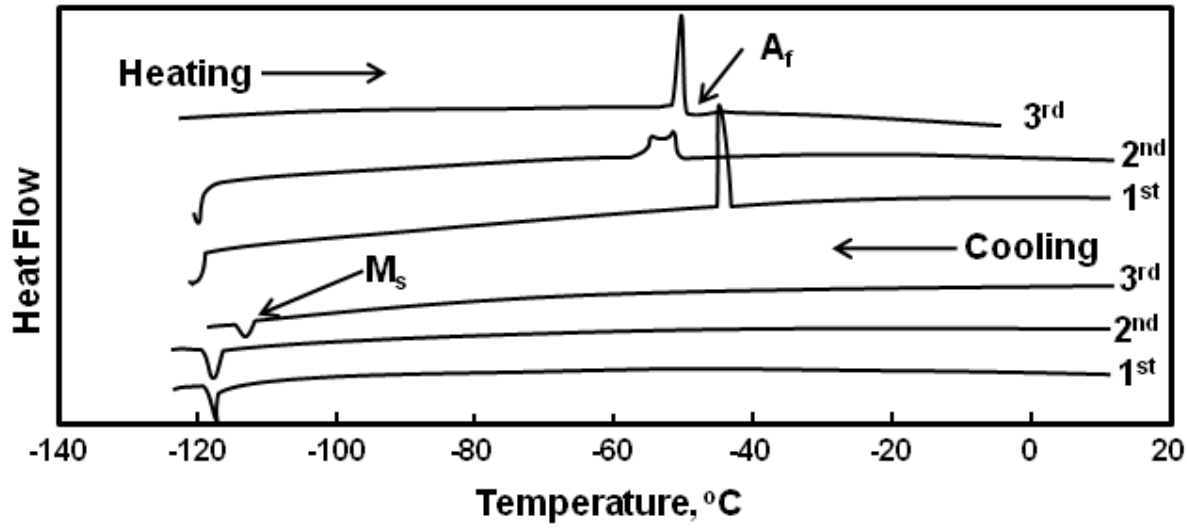

Figure 6 - Representative DSC results for a candidate FSMA composition showing the austenite finish temperature (A_f) and the martensite start temperature (M_s).

Figure 7 shows typical acoustic emission responses for a) a structural material (Al alloy) and b) a shape-memory alloy under increasing strain. The number of acoustic emission responses and the amplitude of the responses is greater for the FSMA than for the structural material. For this particular test, 5% of the emissions for the FSMA had amplitudes more than an order of magnitude greater than those for the aluminum.

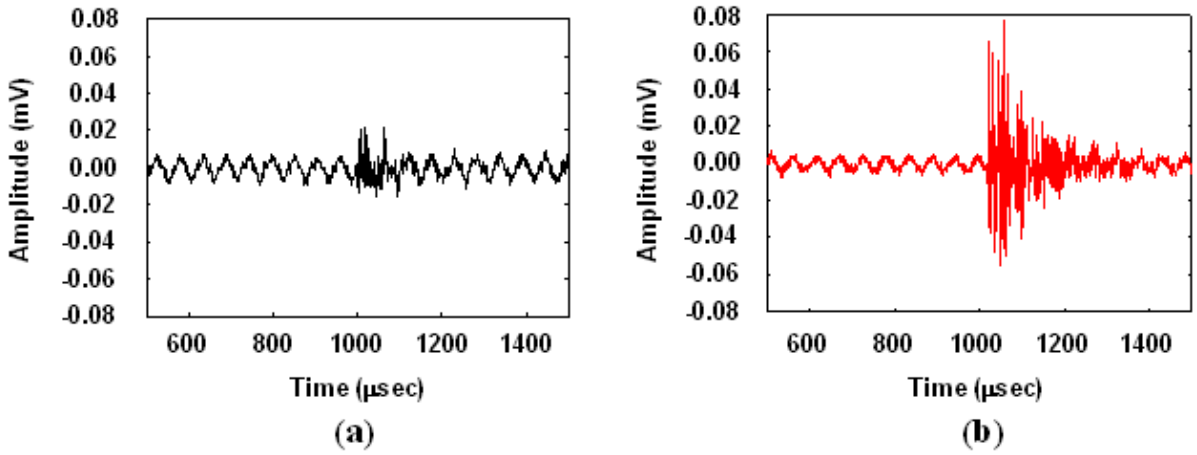

Figure 7 - Typical acoustic emission responses for (a) a structural material (Al alloy) and (b) a shape-memory material under increasing strain.

The raw GMR response from the compression test procedure are plotted as a function of the stroke and is presented in Figure 8. Because the platens move relative to the GMR sensor, baseline tests of the GMR response to the platens and surrounding environment were needed. This particular test series had two baselines collected: air (no specimen but platens moved through space) and an aluminum specimen was compressed. The active FSMA response deviation from the baselines is readily observed in Figure 8 as the stroke or strain is increased above approximately 0.06 mm stroke. This FSMA concept provides two NDE responses to characterize damage (AE and GMR).

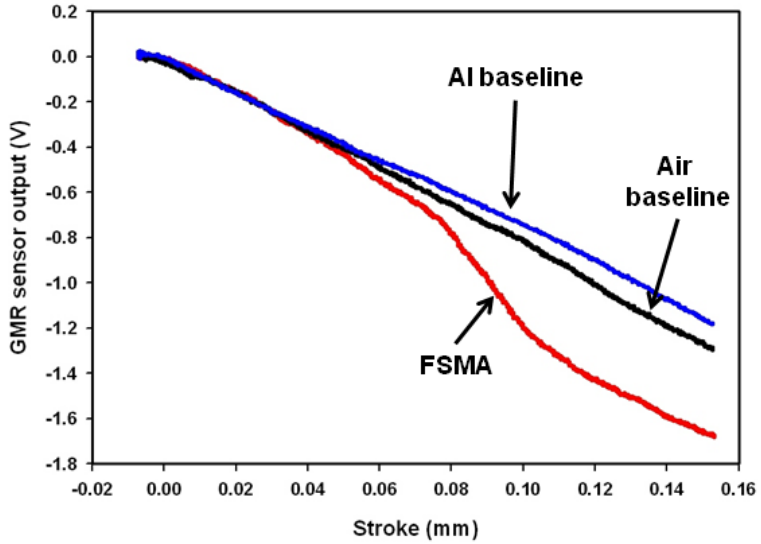

Figure 8 - GMR response of shape memory material with increasing strain.

Behavior of Embedded Sensory Particles

For the first generation of sensory alloys, CoNiAl FSMA was first solution treated and quenched to retain the austenite phase and then mechanically fragmented to produce sensory particles. The sensory alloy was then produced by incorporating the particles into aluminum by vacuum bagging both the sensory particles and aluminum powder and then hot rolling. Figure 9a shows an optical micrograph of the cross-section of the resulting panel. The consolidation process produced good consolidation through the thickness, however the particles are large, up to 1 mm in length, and irregularly shaped.

For the second generation of the sensory alloys, powder was produced using gas atomization. This process produced much finer spherical particles on the order of 10 to 50 μm. The sensory alloy was then fabricated by consolidating the sensory particles and aluminum powder by vacuum hot press. In order to examine the effect of consolidation times, panels were held in the vacuum hot press for either 15 min or 60 min. Figure 9b shows a micrograph of a resulting sensory alloy panel produced by vacuum hot press after a consolidation of 15 min. Examination of the panels consolidated for 60 min revealed the formation of large Al-rich diffusion zones between the matrix and particles that were between 10 and 30 μm.

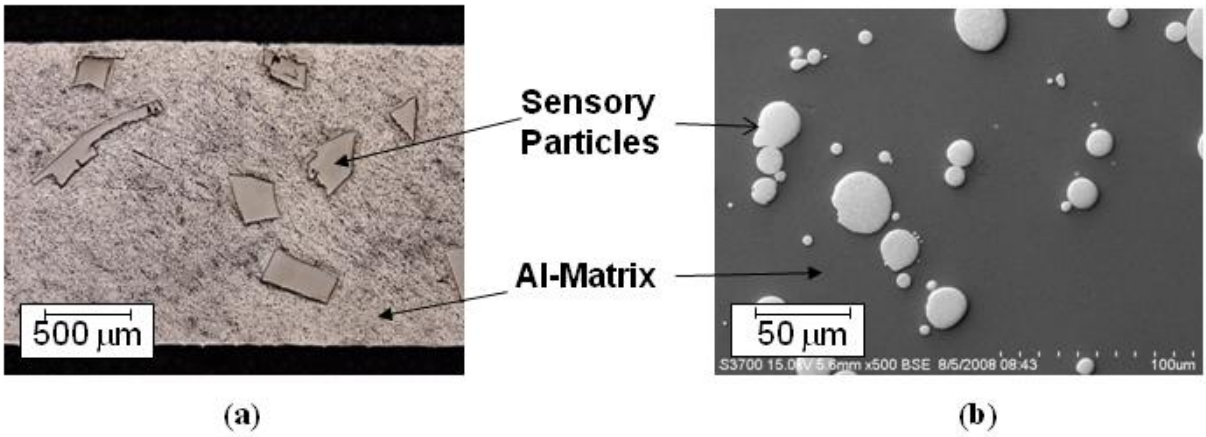

Figure 9 - Micrographs of sensory alloys fabricated using (a) mechanically fragmented CoNiAl FSMA and (b) gas atomized CoNiAl FSMA powder.

The NDE response of the sensory alloys was evaluated, and the results are shown in Figure 10. This plot shows both the AE and GMR of the embedded shape memory particles versus stroke or displacement of the compression platens. The symbols used to represent the AE response indicate each AE event measured during the compression loading. The GMR response is plotted as the change in GMR response from the response of the air baseline, which is denoted as ΔGMR. A third curve in Figure 10 represents the load versus stroke data. There is a significant change in the slope of the ΔGMR response just before the onset of significant plasticity (as noted by the change in slope for the load versus stroke curve) in the aluminum matrix. Changes in the AE rate are also seen by a distinct change in slope evident just after the onset of plasticity and extending until just before final fracture. Although this slopechange is presumably due to the shape memory transition, the fact that it occurs over a range of strain values suggests that the chemistry of the FSMA particles may not be uniform. Also, note that the change in slopes for AE and ΔGMR measurements are at different stroke values suggesting

that the composition is not fully optimized and the magnetic and phase changes are not occurring at the same strain.

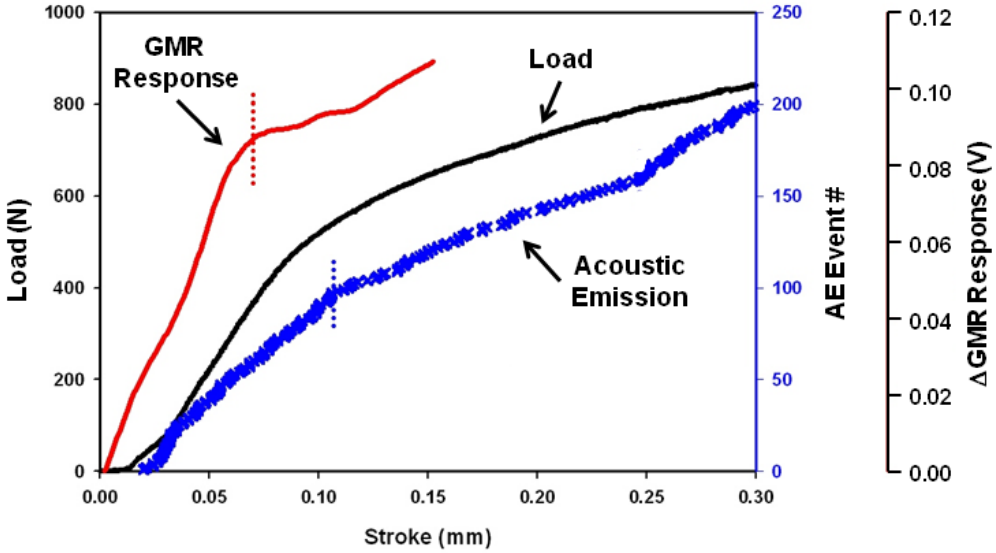

Figure 10 - AE and GMR response of sensory alloy with increasing strain.

The tensile and fatigue behavior of the sensory alloys were characterized to evaluate the impact of the sensory particles on the mechanical properties. Panels were produced using the vacuum hot press from pure aluminum powder (matrix) and gas atomized CoNiAl sensory particles. Also, panels were produced without particles using the same process. In addition, the effect of the consolidation parameters were evaluated by varying the consolidation times (15 or 60 minutes) for the panels. Specimens were machined from these panels, and the resulting tensile and fatigue data are shown in Figure 11.

Data for the pure aluminum specimen with a 15 min and 60 min consolidation time are shown as the solid and dashed curve, respectively, in Figure 11a. Both consolidation times produced an ultimate stress of approximately 84.8 MPa with good ductility. In both cases, determination of elongation at failure was not possible as failure occurred at a strain greater than 25%, which is the capacity of the displacement gages used. These results suggest that for the panels produced with Al powder, varying the consolidation time has no apparent effect on the tensile properties.

The addition of particles resulted in reduction of ductility and increases in strength. For the sensory alloy panels consolidated for 15 min (dotted curve), the elongation at failure was approximately 2.7%. The ultimate stress observed was 101 MPa (approximately a 19% increase over the baseline), which occurred at a strain of approximately 1.4% (approximately a factor of 12 reduction in ductility). For the sensory alloy panels consolidated for 60 min (dash-dot-dot curve), the elongation at failure was approximately 14.7%. The ultimate stress observed was 95.8 MPa (nearly a 13% increase over the baseline), which occurred at a strain of approximately 8.7% (nearly a factor of 3 reduction in ductility). For the SMA alloy tested (hard particle embedded in a relatively soft matrix), the addition of the sensory particles increased the strength at the expense of ductility. The diffusion zones formed by the 60 min consolidation resulted in recovery of much of the lost ductility.

The fatigue data are plotted in Figure 11b for all four panel types; closed and open symbols are for panels with and without particles, respectively, and circular and triangular symbols are for panels with short and long consolidation times, respectively. Here, the fatigue data show a trend that as maximum stress decreases from approximately 85 MPa to 60 MPa, fatigue life increases from approximately 10^3 to 10^7 cycles. Little differences in the fatigue life data are seen between data sets, suggesting that neither the presence of particles nor diffusion zones has a significant effect on the fatigue performance of these sensory alloys.

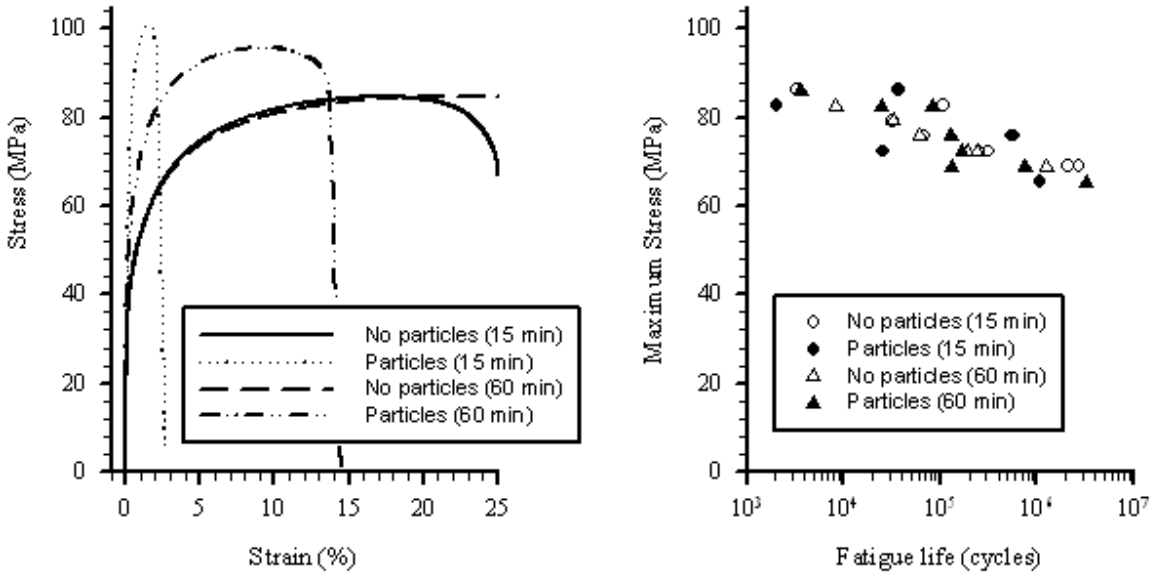

(a) Tensile data (b) Fatigue data

Figure 11 - Mechanical test data for particles embedded in a pure aluminum matrix.

Conclusions

Sensory alloys were successfully fabricated consisting of sensory particles with an enhanced NDE response to damage processes compared to that of structural aluminum. These alloys were tested under increasing strain and showed both AE and magnetic responses. In addition, mechanical testing revealed that the presence of the particles did not adversely affect the fatigue properties of the resulting sensory alloys. The presence of the particles increased the tensile strength of the aluminum sensory alloys, but at the expense of ductility. By changing the processing condition, increasing consolidation time resulting in increased diffusion zones and much of this lost ductility is recovered, suggesting that structural alloys can be fabricated with sensory particles to improve the ability to measure damage using traditional NDE tools.

References

[1] K. Otsuka, *Shape Memory Materials,* Cambridge University Press, 1998

[2] S. Takahashi and Y. Umahoshi, *J. Phys.: Cons. Matter*, Vol. 2, 1990, p 4007

[3] H. Morito, A. Fujita, K. Fukamichi, R. Kainuma, and I. Ishida, *Appl. Phys. Lett*., Vol 81, 2002, p 1657

[4] R. Kainuma, M. Ise, C.-C. Jia, H. Ohtani and K. Ishida, *Intermetallics*, Vol 4, 1996, p S151

[5] K. Oikawa, L. Wulff, T. Iijima, F. Gejima, T. Ohmori, A. Fujita, K. Fukamichi, R. Kainuma, and K. Ishida, *Appl. Phys. Lett*., Vol 79, 2001, p 290

[6] Z. H. Liu, X. F. Dai, Z. Y. Zhu, H. N. Hu, J. L. Chen, G. D. Liu and G. H Wu, *J. Phys. D*: *Appl. Phys.*, Vol. 37, 2004, p 2643

[7] K. Ullakko, J. K. Huang, C. Kanter, V. V. Kokorin, and R. C. O'Handley, *Appl. Phys. Lett*. Vol 69, 1996, p 1966

[8] S. J. Murray, M. Marioni, A. Kukla, J. Robinson, R. C. O'Handley, and S. M. Allen, *J. Appl. Phys*., Vol 87, 2000, p 5774

[9] S. J. Murray, M. Marioni, S. M. Allen, and R. C. O'Handley, *Appl. Phys. Lett*., Vol 77, 2000, p 886

[10] F. Gejima, Y. Sutou, R. Kainuma, and K. Ishida, *Metall. Mater. Trans. A*, Vol 30A, 1999, p 2721

[11] R. Kainuma, F. Gejima, Y. Sutou, I. Ohnuma, and K. Ishida, *Mater. Trans., JIM*, Vol 41, 2000, p 943

[12] Fujita, K. Fukamichi, F. Gejima, R. Kainuma, and K. Ishida, *Appl. Phys*. Lett., Vol 77, 2000, p 3054

[13] R. D. James and M. Wuttig, *Philos. Mag. A*, Vol 77, 1998, p 1273

[14] Y. Furuya, N. W. Hagood, H. Kimura, and T. Watanabe, *Mater. Trans., JIM*, Vol 39, 1998, p 1248

[15] T. Kakeshita, T. Takeuchi, T. Fukuda, T. Saburi, R. Oshima, S. Muto, and K. Kishio, *Mater. Trans., JIM,* Vol 41, 2000, p 882

[16] ASTM Standard E 466, "Standard Practice for Conducting Force Controlled Constant Amplitude Axial Fatigue Tests of Metallic Materials," Annual Book of ASTM Standards, Vol. 3.01, West Conshohocken, PA, 2006

[17] ASTM Standard E 8, "Standard Test Methods for Tension Testing of Metallic Materials," Annual Book of ASTM Standards, Vol. 3.01, West Conshohocken, PA, 2006